Supplementary Information (SI) for Energy & Environmental Science.

Supplementary information

Electrical power generation from asymmetric greenhouse gas capture

Tae Gwang Yun, †*[b] Yejin Lee, †[a, c] Joonchul Shin, †[d] Dong Ho Lee, [e] Min Taek Hong, [e] Seonghun Lee, [b] Sang-Joon Kim, [f] Hyun Ji Lee, [l] Jiwon Lee, [g, h] Gyeongrok Min, [g, i] Seunghyun Weon, [m, n] Minho Choi, [m, n] Ho Won Jang, [c, o] Han Seul Kim, *[e, j, k] and Ji-Soo Jang, *[a,p]

[a] Electronic and Hybrid Materials Research Center, Korea Institute of Science and Technology (KIST); Seoul, 02792, Republic of Korea.

[b] Department of Molecular Science and Technology, Ajou University; Suwon, 16499, Republic of Korea.

[c] Department of Materials Science and Engineering, Research Institute of Advanced Materials, Seoul National University; Seoul, 08826, Republic of Korea.

[d] Advanced Bio and Healthcare Materials Research Division, Korea Institute of Materials Science (KIMS), Changwon, Republic of Korea

[e] Department of Advanced Materials Engineering, Chungbuk National University; Cheongju, 28644, Republic of Korea

[f] Korea Department of Materials Science and Engineering, Chungnam National University, Daejeon 34134, Republic of Korea

[g] Center for Climate and Carbon Cycle Research, Korea Institute of Science and Technology (KIST), Seoul, 02792, Republic of Korea

[h] Division of Energy & Environment Technology, KIST School, University of Science and Technology, Seoul, 02792, Republic of Korea

[i] Department of Materials Science and Engineering, Korea University, Seoul 02841, Republic of Korea

[j] Department of Urban, Energy, Environmental Engineering, Chungbuk National University; Cheongju, 28644, Republic of Korea

[k]Advanced Energy Research Institute, Chungbuk National University, Chungdae-ro 1, Seowon-Gu, Cheongju, Chungbuk, 28644, Republic of Korea

[l]CO_2 & Energy Research Center, Korea Research Institute of Chemical Technology (KRICT), Daejeon 34114, Republic of Korea

[m] School of Health and Environmental Science & Department of Health and Safety Convergence Science, Korea University, Seoul 02841, Republic of Korea.

[n] Transdisciplinary Major in Learning Health Systems, Graduate School, Korea University, 145 Anam-Ro, Seoul 02841, Republic of Korea.

[o]Advanced Institute of Convergence Technology, Seoul National University, Suwon 16229, Republic of Korea

p.SKKU Advanced Institute of Nanotechnology and Department of Nanoengineering,Sungkyunkwan University, Suwon 16419, Republic of Korea

*Corresponding author. Email: wkdwltn92@skku.edu, ytk0402@ajou.ac.kr, hanseul.kim@chungbuk.ac.kr

†These authors contributed equally to this work

Table of Contents

Supplementary Figures

Figure S1 | SEM images.
Figure S2 | Experimental setup for gas adsorption evaluation.
Figure S3 | DRIFTS spectra of the polyacrylamide hydrogel.
Figure S4 | Long-term voltage stability of the GCEG.
Figure S5 | Cyclic adsorption–desorption stability of the GCEG.
Figure S6 | Temperature-dependent V_{OC} response of the GCEG.
Figure S7 | Nyquist plots of the GCEG under NO_2 exposure.
Figure S8 | Diffusion coefficient and ion mobility of the GCEG.
Figure S9 | Spin-resolved PDOS of gas-adsorbed PAM hydrogels.
Figure S10 | Net electron count and Fermi-level shift upon gas adsorption.
Figure S11 | Experimental setup for gas energy harvesting measurements.
Figure S12 | Low-concentration NO_2 response of the GCEG.
Figure S13 | Voltage output under varying load resistances.
Figure S14 | Power output dependence on NO_2 concentration at 80% RH.
Figure S15 | Electrical performance of the GCEG with alternative solutions.
Figure S16 | Series and parallel connection performance of the GCEG.
Figure S17 | Electrical performance of the GCEG under CO_2 exposure.
Figure S18 | V_{OC} profiles of the modified GCEG with amine solutions.
Figure S19 | Long-term CO_2 response of the modified GCEG.
Figure S20 | Cyclic CO_2 response of the modified GCEG.
Figure S21 | Gas adsorption capacities of bare, PAM, and PAM+DEA.
Figure S22 | Digital images of conductive coatings on mulberry paper.
Figure S23 | Electrical performance with different conductive coatings.
Figure S24 | IoT sensor demonstration powered by the GCEG array.
Figure S25 | Outdoor performance evaluation of the GCEG.
Figure S26 | Mechanical durability under cyclic bending.
Figure S27 | Effect of LiCl concentration on electrical output.
Figure S28 | Electrical performance with gelatin-based hydrogels.
Figure S29 | Electrical output as a function of hydrogel weight.
Figure S30 | Electrical performance with PEDOT:PSS/carbon black coating.
Figure S31 | Series–parallel enhancement under CO_2 exposure.
Figure S32 | Adsorption kinetics and recovery behavior under NO_2 exposure.

Supplementary Tables

Table S1 | Comparison of electrical performance with other energy harvesting devices based on electrical double layers.
Table S2 | Comparison of NO_2 adsorption capacities with other materials.
Table S3 | Parameters for calculating gas adsorption capacities.

Supplementary Discussion

Discussion S1 | Calculation of gas adsorption capacities.

References

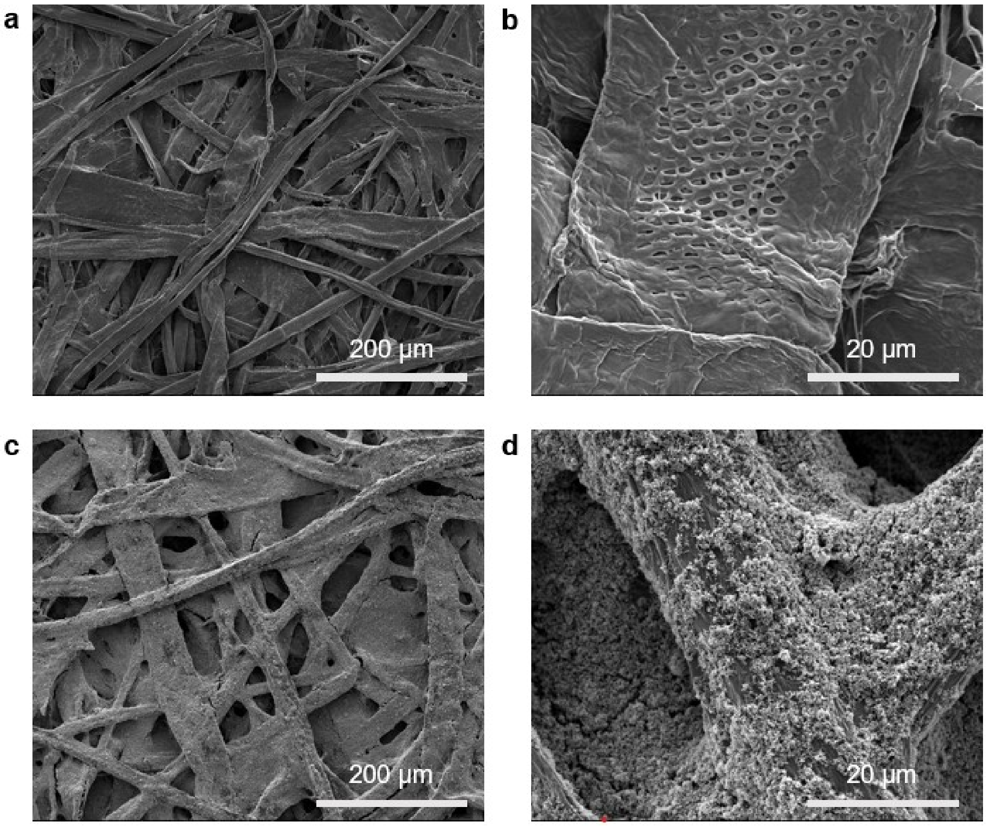

Figure S1. SEM images of pristine mulberry paper (a, b) and carbon black-coated mulberry paper (c, d).

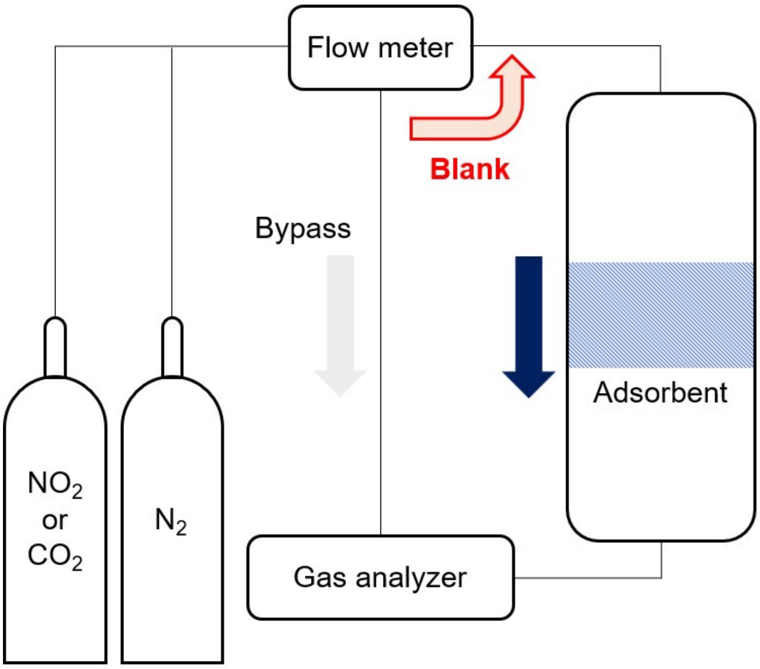

Figure S2. Schematic of the experimental setup for evaluating gas adsorption performance.

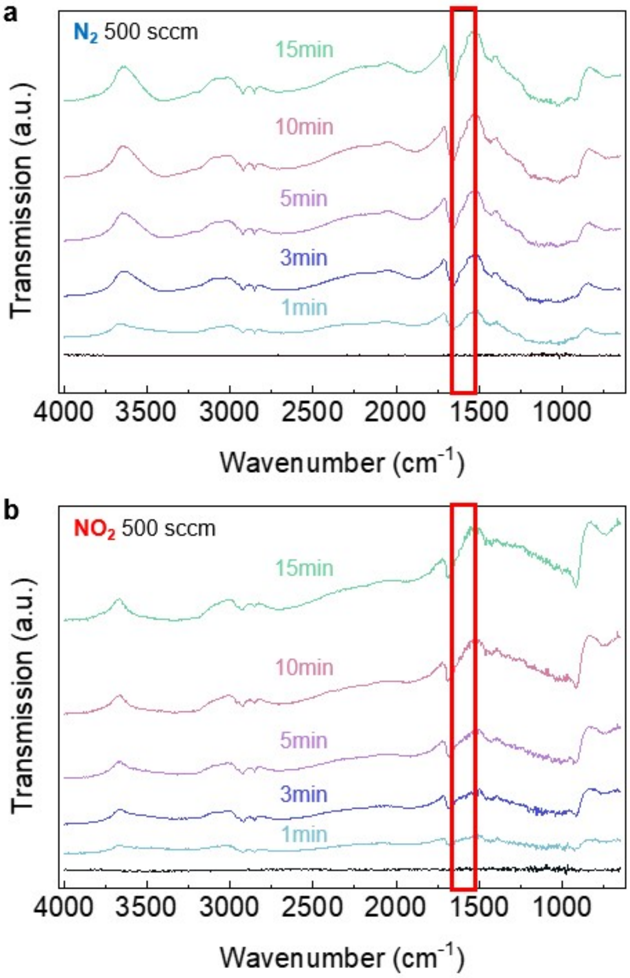

Figure S3. Diffuse Reflectance Infrared Fourier Transform Spectroscopy (DRIFTS) spectra of the polyacrylamide hydrogel recorded 15 min after exposure to (a) N_2 and (b) 1000 ppm NO_2 at 0% RH and room temperature.

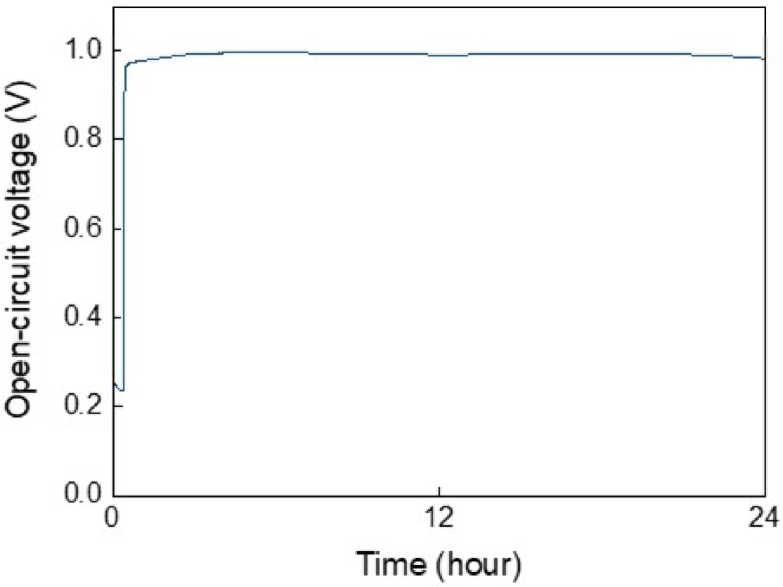

Figure S4. Long-term voltage stability of the GCEG under continuous exposure to 50 ppm NO_2 at 30% RH.

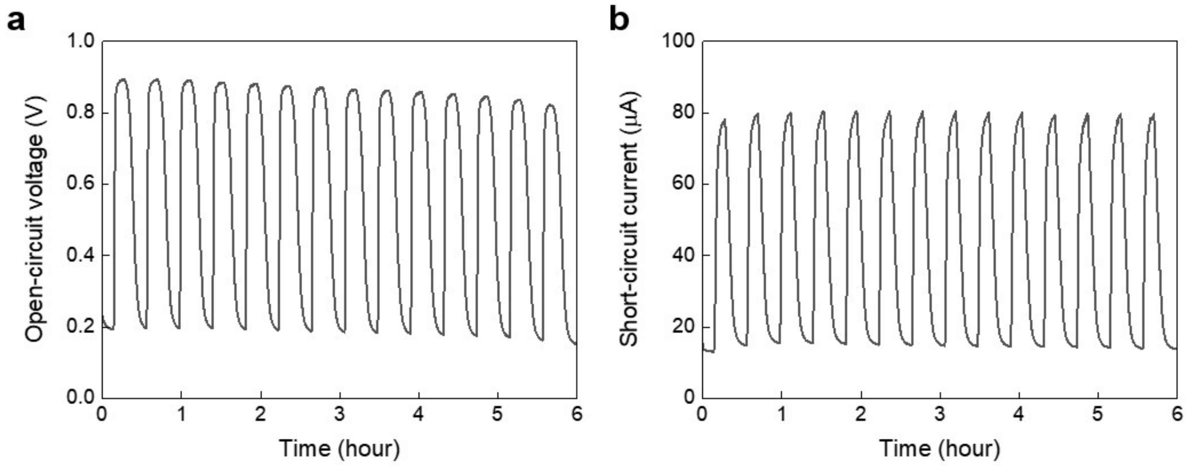

Figure S5. (A) V_{OC} and (B) I_{SC} of the GCEG over 15 consecutive adsorption–desorption cycles under 30 ppm NO_2 exposure at 30% RH.

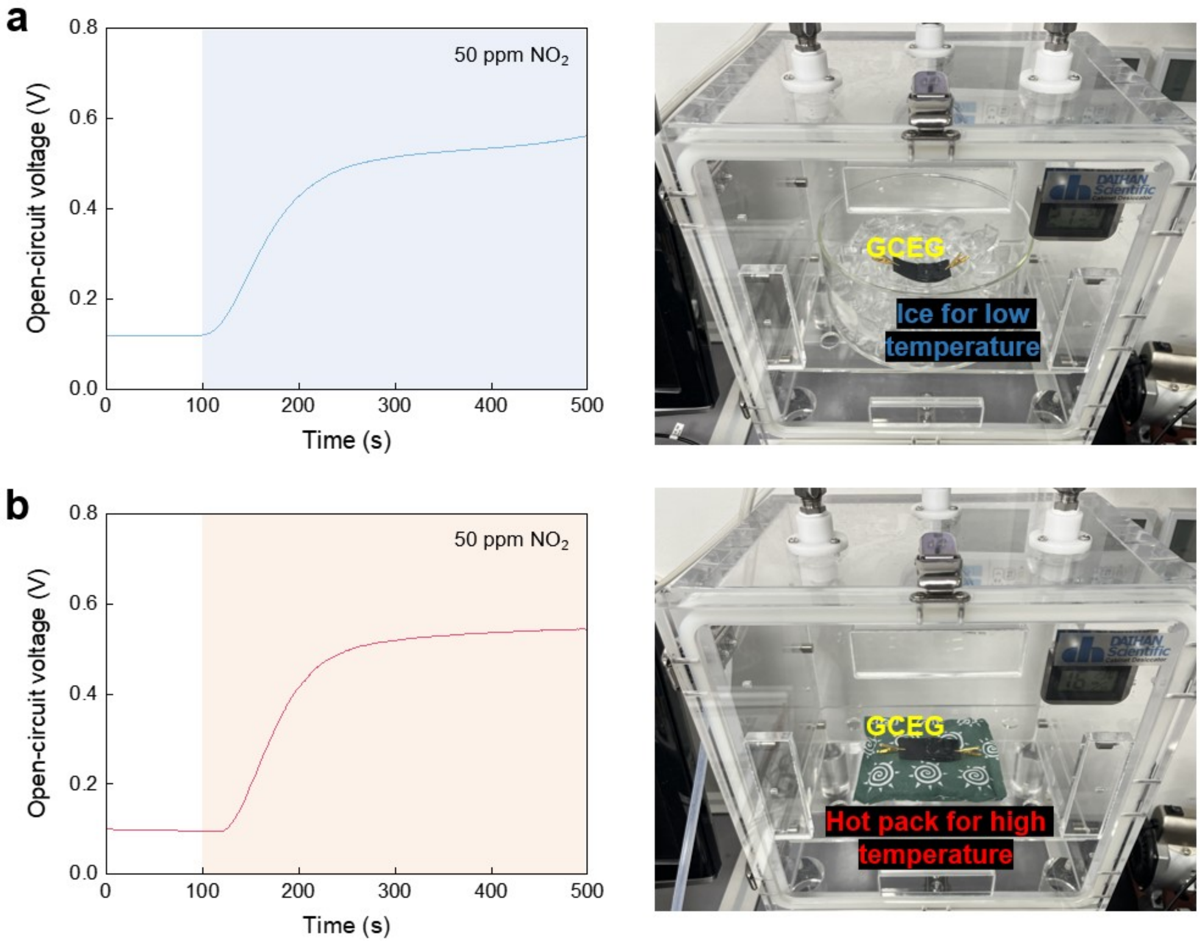

Figure S6. Measured V_{OC} of the GCEG exposed to 50 ppm NO_2 at 0% RH under different temperature conditions and digital images of the experimental setup at (a) cold and (b) hot temperature.

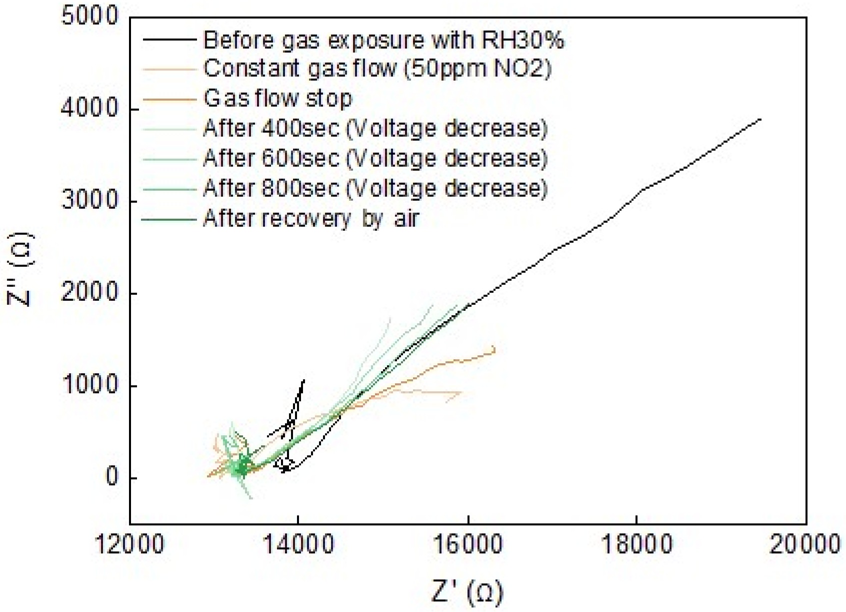

Figure S7. Nyquist plots of the GCEG upon exposure to 50 ppm NO_2 gas, obtained from in situ electrochemical impedance spectroscopy (EIS) analysis. All measurements were performed at 30% RH and room temperature.

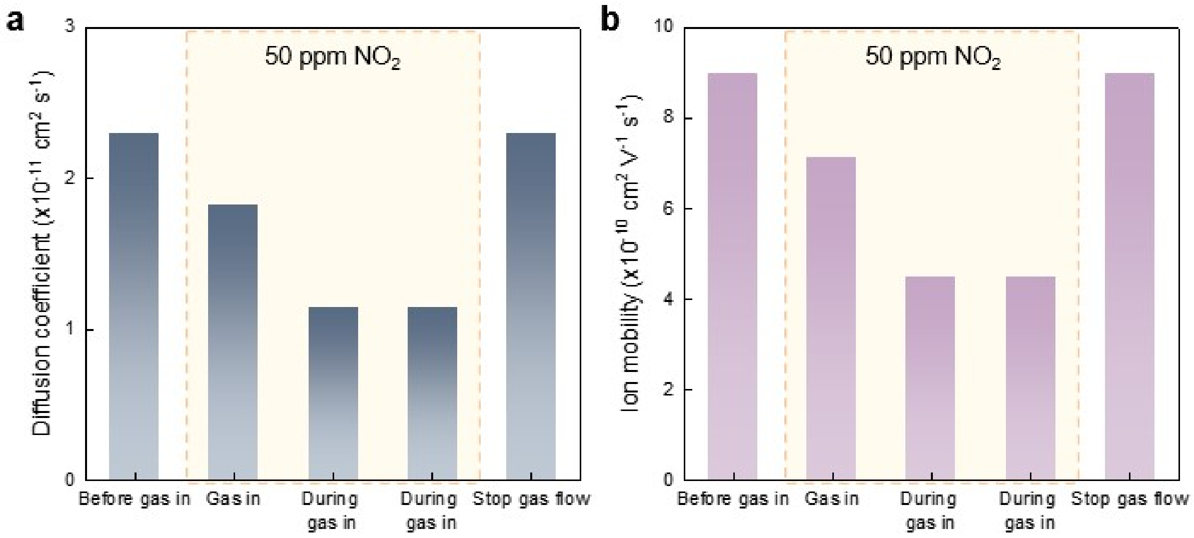

Figure S8. Changes in diffusion coefficient and ion mobility of the GCEG under exposure to NO_2 gas. (a) Diffusion coefficient and (b) ion mobility of the GCEG exposed to 50 ppm NO_2 gas, obtained from in situ electrochemical impedance spectroscopy (EIS) analysis. All measurements were performed at 30% RH and room temperature.

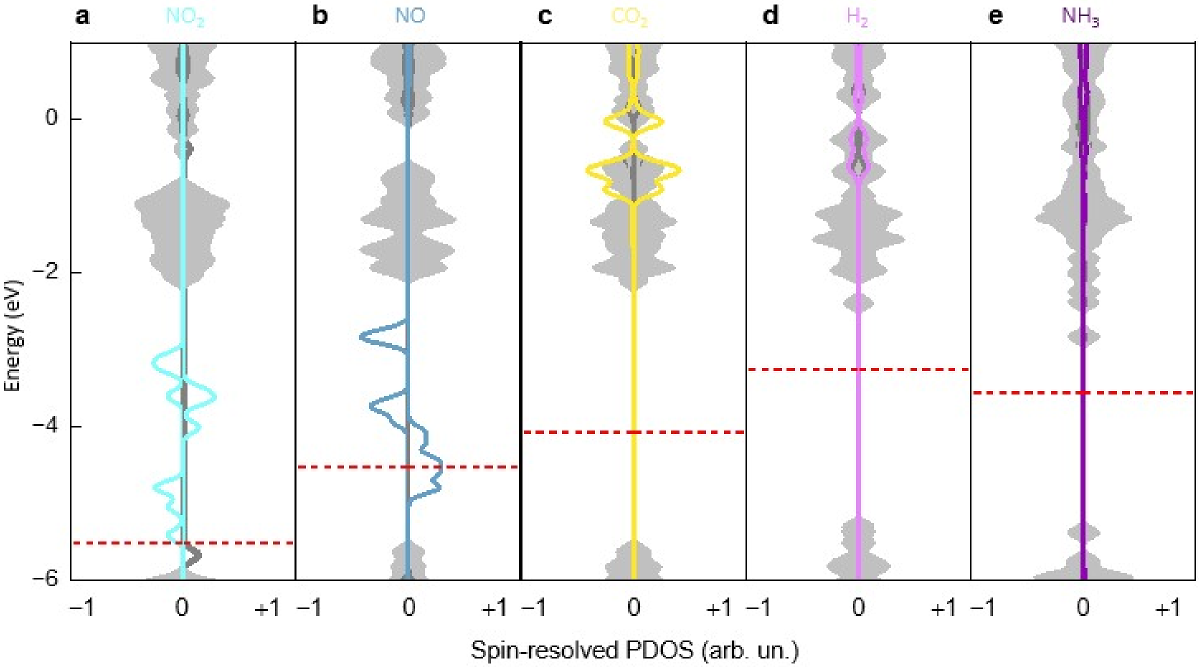

Figure S9. Spin-resolved PDOS plots of gas-adsorbed PAM hydrogel systems under dry (non-hydrated) conditions for (a) NO_2, (b) NO, (c) CO_2, (d) H_2, and (e) NH_3 molecules. Positive and negative values indicate the magnitude of DOS for up and down electronic spins, respectively.

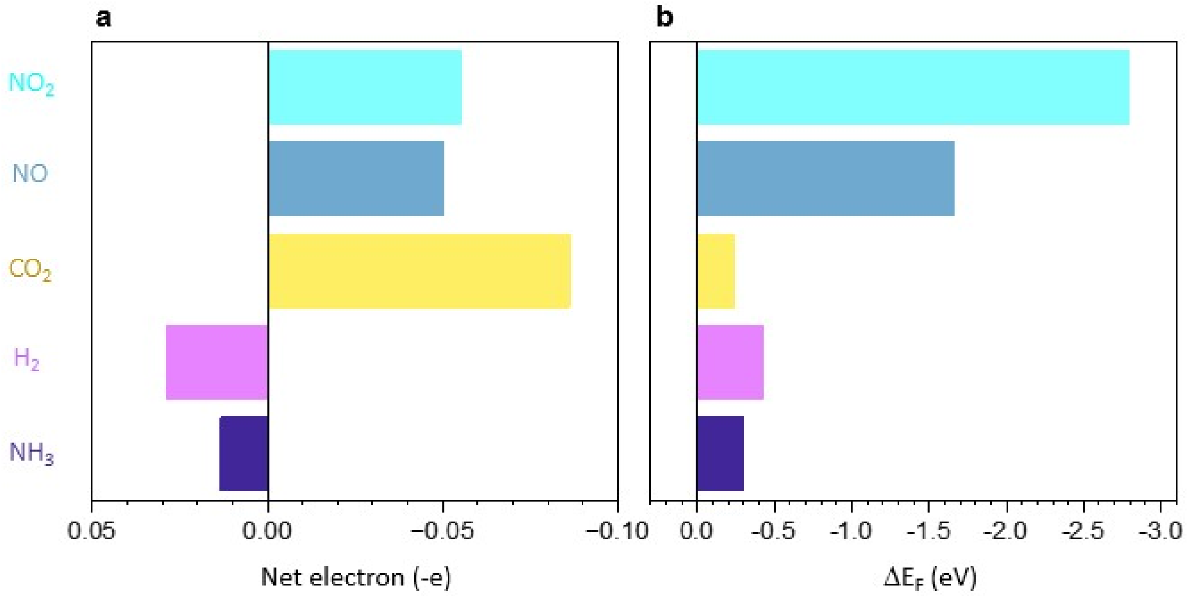

Figure S10. (a) Change in the net electron count and (b) ΔE_F associated with each gas molecule within the system in dry (non-hydrated) conditions.

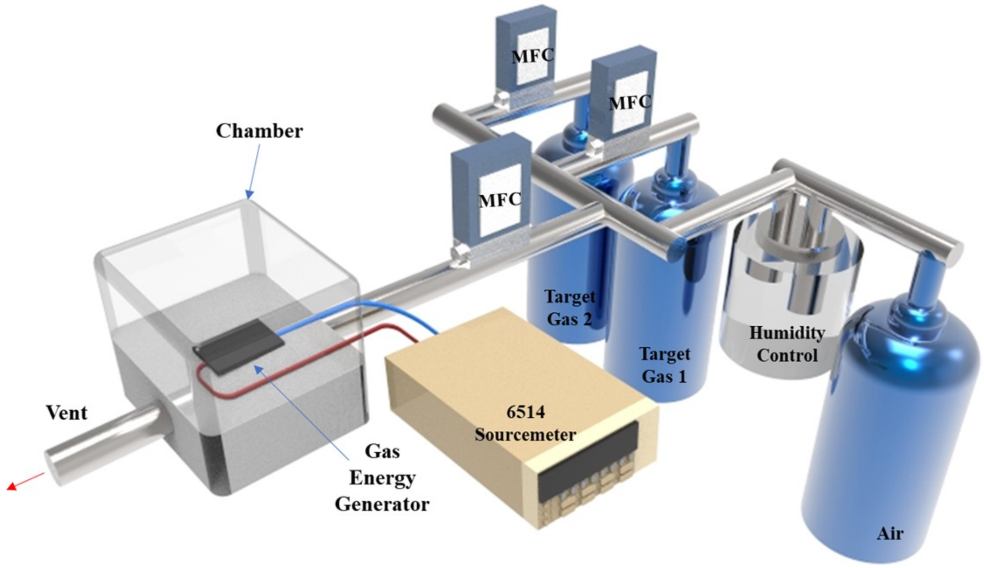

Figure S11. Schematic of the experimental setup for gas energy harvesting measurements.

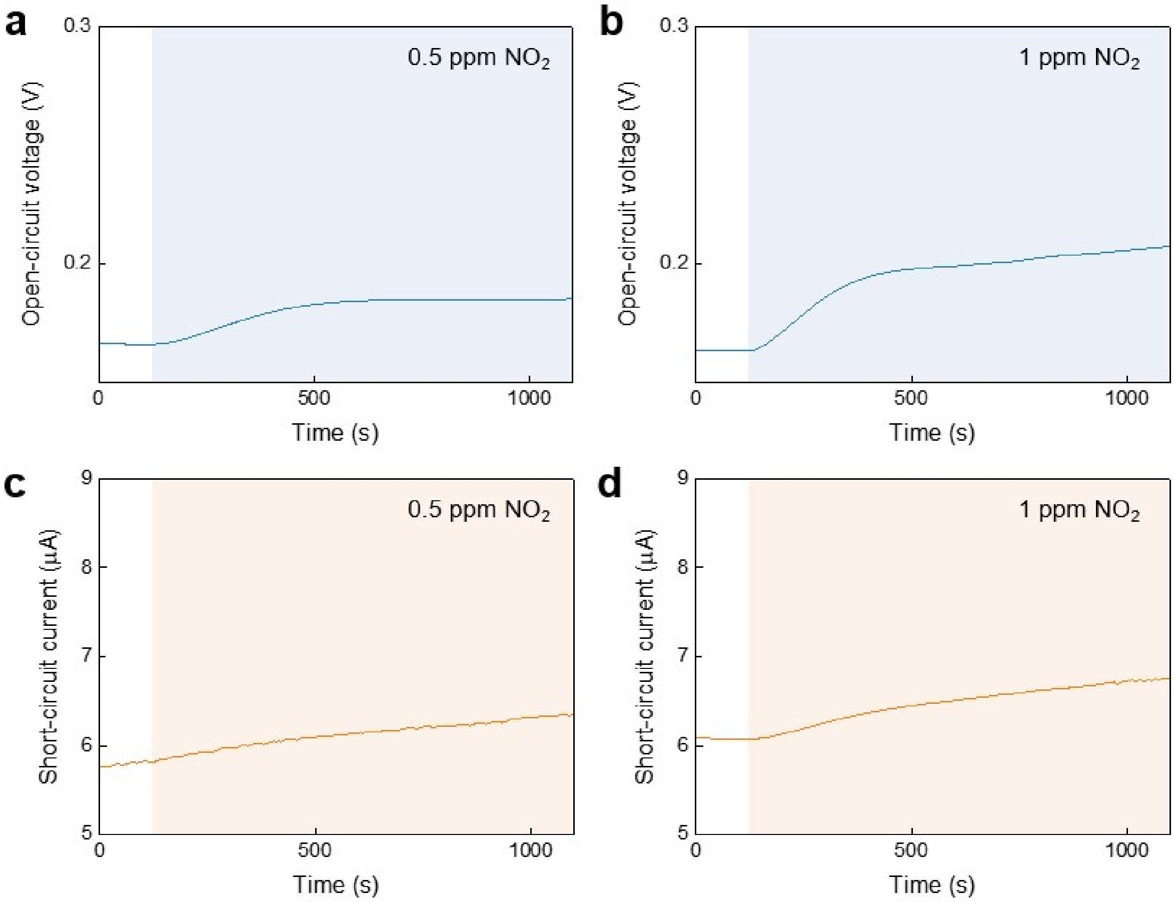

Figure S12. Measured V_{OC} of the GCEG under (a) 0.5 ppm NO_2 exposure and (b) 1 ppm NO_2 exposure, and I_{SC} under (c) 0.5 ppm NO_2 exposure and (d) 1 ppm NO_2 exposure at 30% RH.

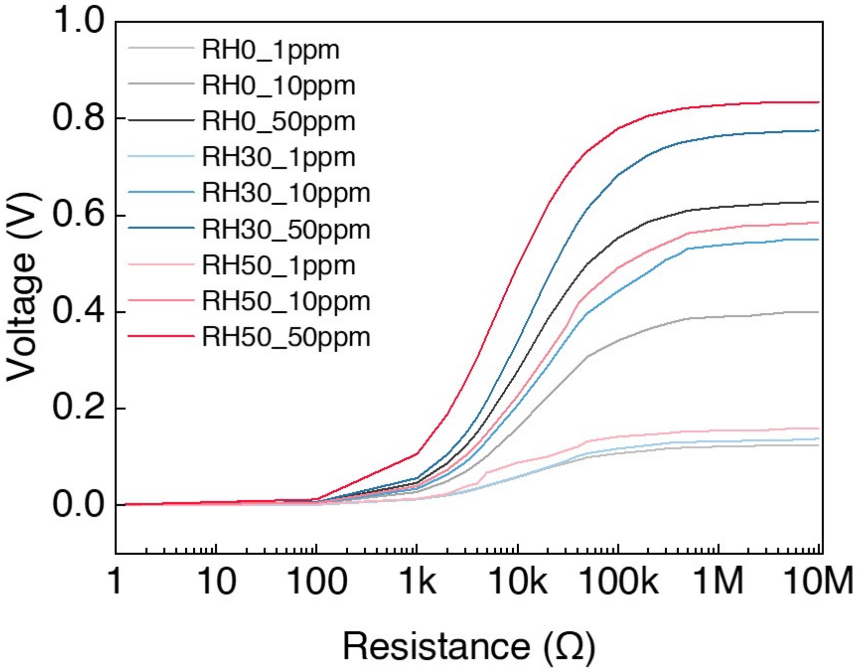

Figure S13. Voltage output of the GCEG across resistances ranging from 1 Ω to 10 MΩ, under varying gas concentrations and RH levels.

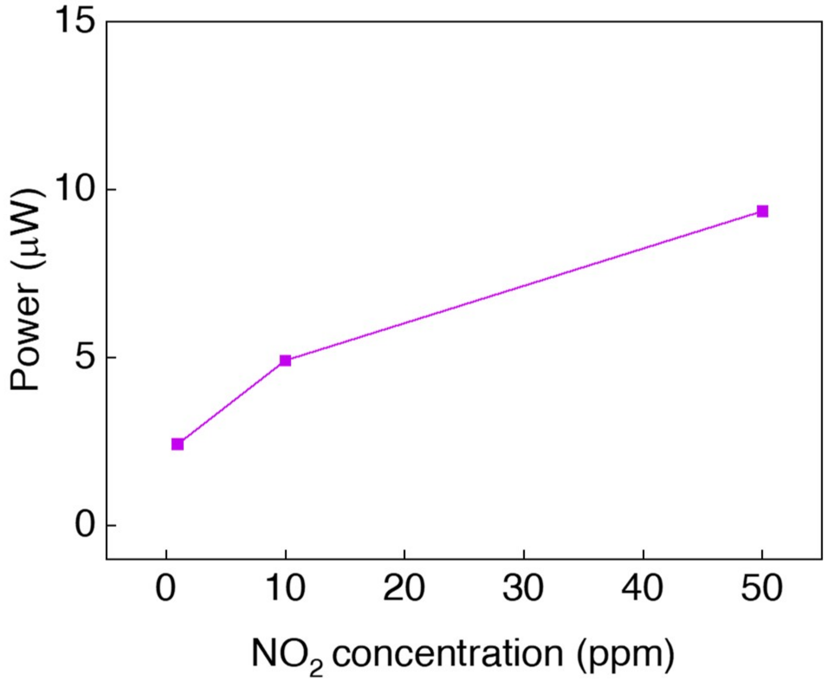

Figure S14. Dependence of the power output on NO_2 concentration at 80% relative humidity.

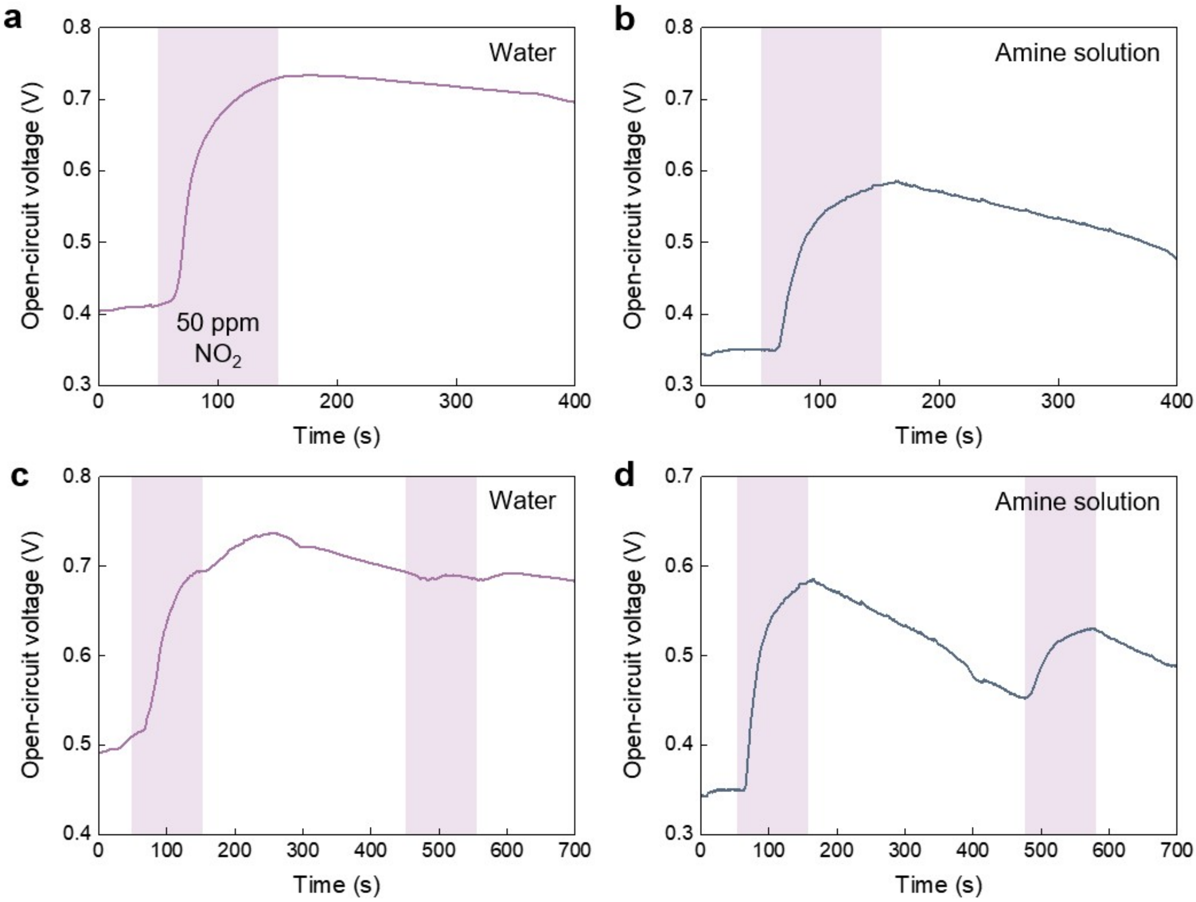

Figure S15. Electrical performance of GCEG with other solutions in place of PAM hydrogel. (a) Measured V_{OC} profiles of the GCEG containing water instead of the PAM hydrogel under exposure to 50 ppm NO_2. (b) Measured V_{OC} profiles of the GCEG containing an amine solution instead of the PAM hydrogel under the same conditions. All measurements were performed at 0% RH and room temperature.

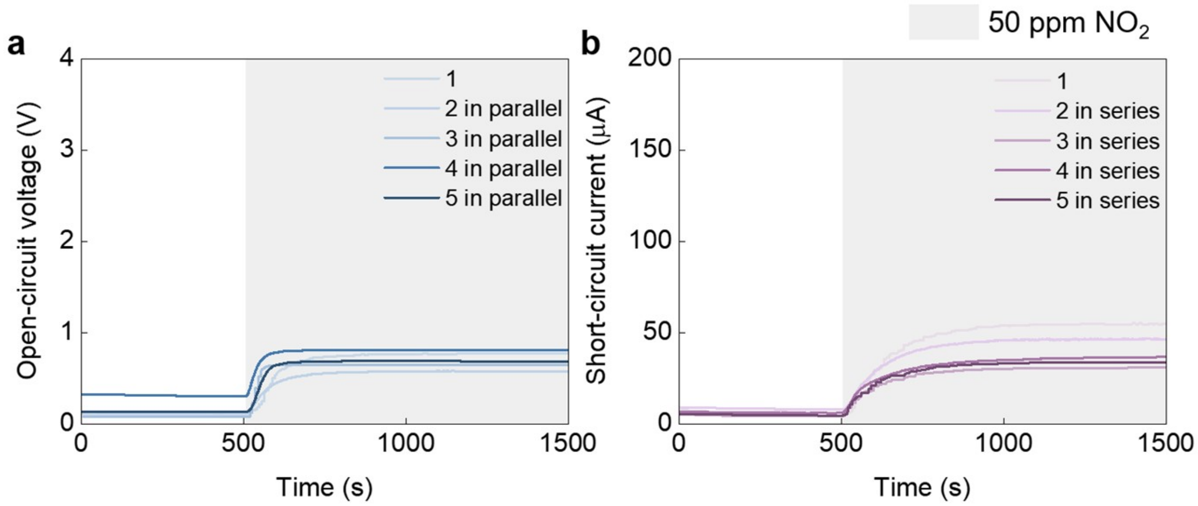

Figure S16. Measured (a) V_{OC} and (b) I_{SC} of the GCEG connected in parallel and series, respectively, under exposure to 50 ppm NO_2.

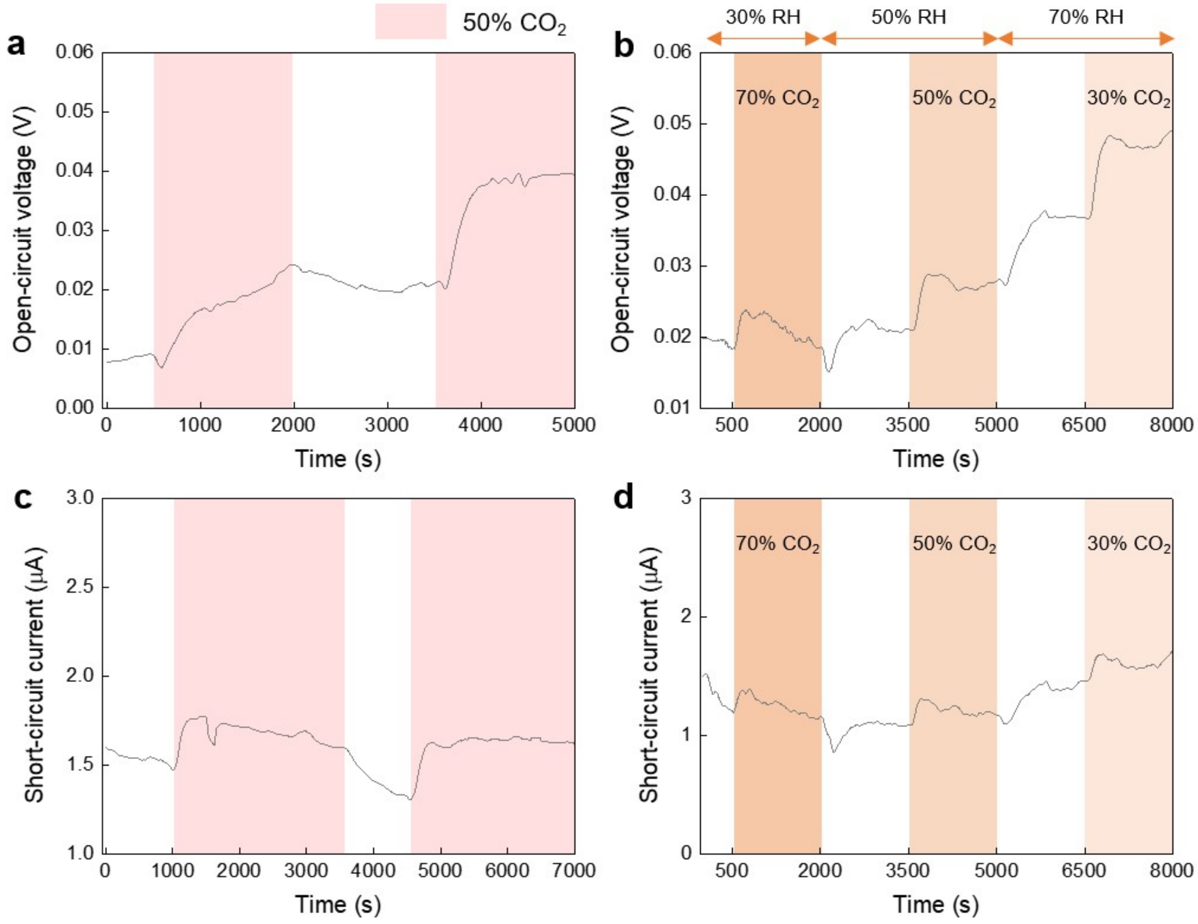

Figure S17. Electrical performance of the GCEG under CO_2 exposure. (a) Measured V_{OC} profiles of the GCEG exposed to 50% CO_2. (b) Measured V_{OC} profiles of the GCEG exposed to 70%, 50%, and 30% CO_2. (c) Measured I_{SC} profiles of the GCEG with exposed to 50% CO_2. (d) Measured I_{SC} profiles of the GCEG exposed to 70%, 50%, and 30% CO_2.

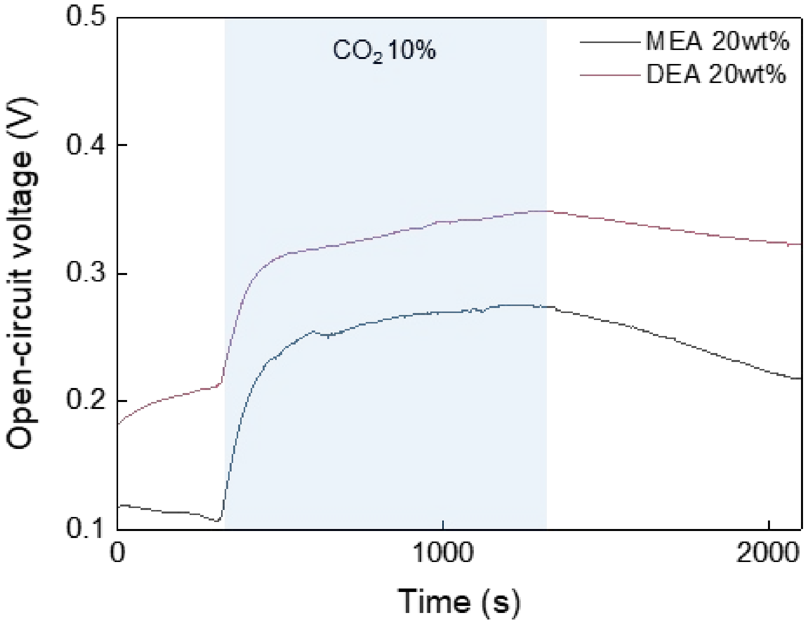

Figure S18. V_{OC} profiles of the modified GCEG incorporating monoethanolamine (MEA) and diethanolamine (DEA) solutions under 10% CO_2 exposure at 30% RH.

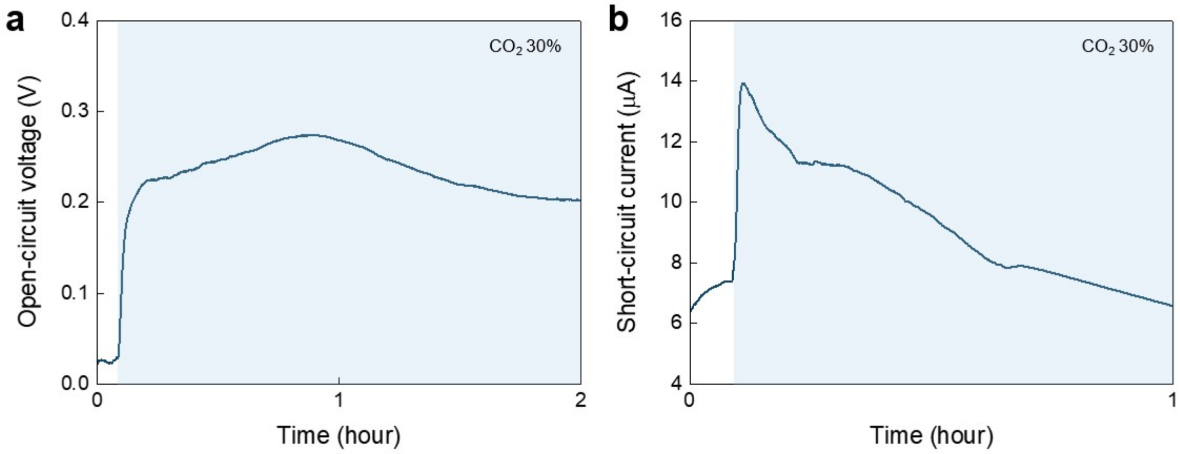

Figure S19. (a) V_{OC} and (b) I_{SC} of the modified GCEG devices under long-term 30% CO_2 exposure at 30% RH.

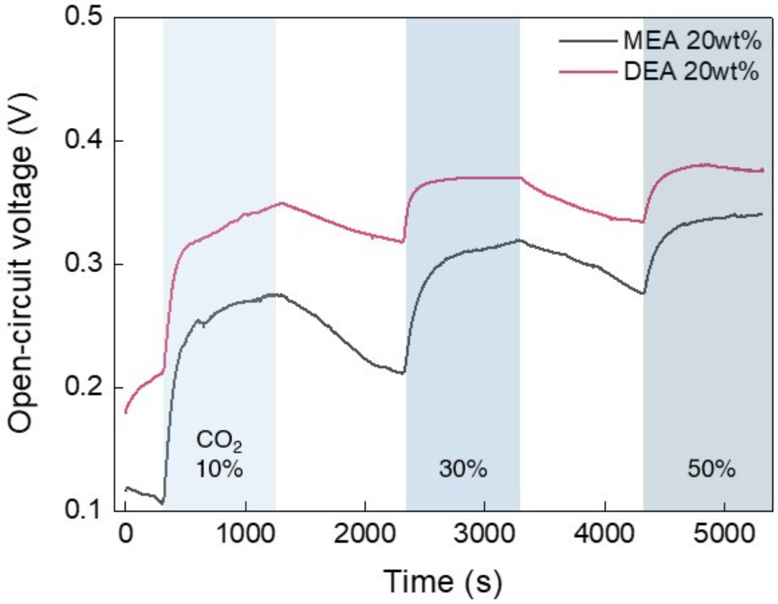

Figure S20. V_{OC} profiles of the modified GCEG devices incorporating monoethanolamine (MEA) and diethanolamine (DEA) solutions under repeated CO_2 exposure at 10%, 30%, and 50% and 30% RH, showing partial recovery of the electrical output upon successive CO_2 adsorption–desorption cycles.

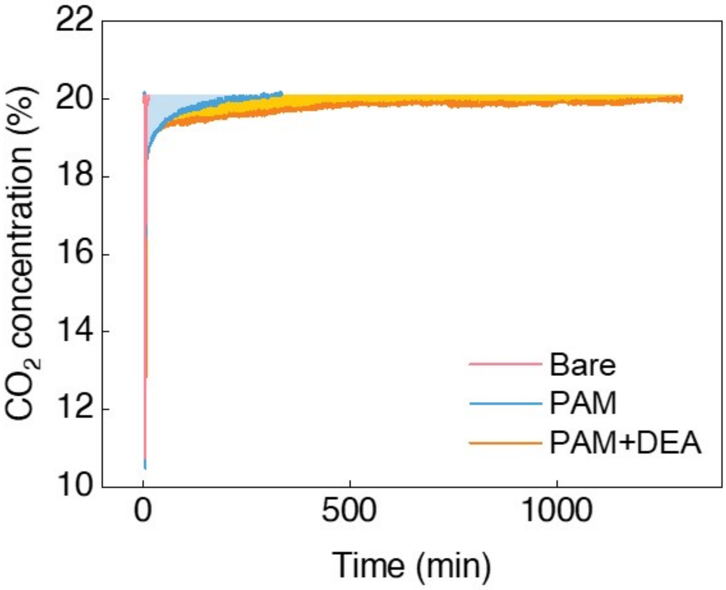

Figure S21. Gas adsorption capacity of the Bare (Carbon black-coated mulberry paper), PAM, and PAM+DEA evaluated under a continuous flow of CO_2.

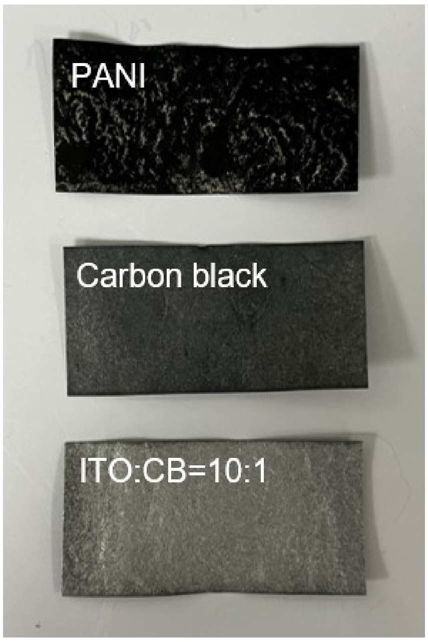

Figure S22. Digital images showing polyaniline, ITO, and carbon black coatings applied on mulberry paper.

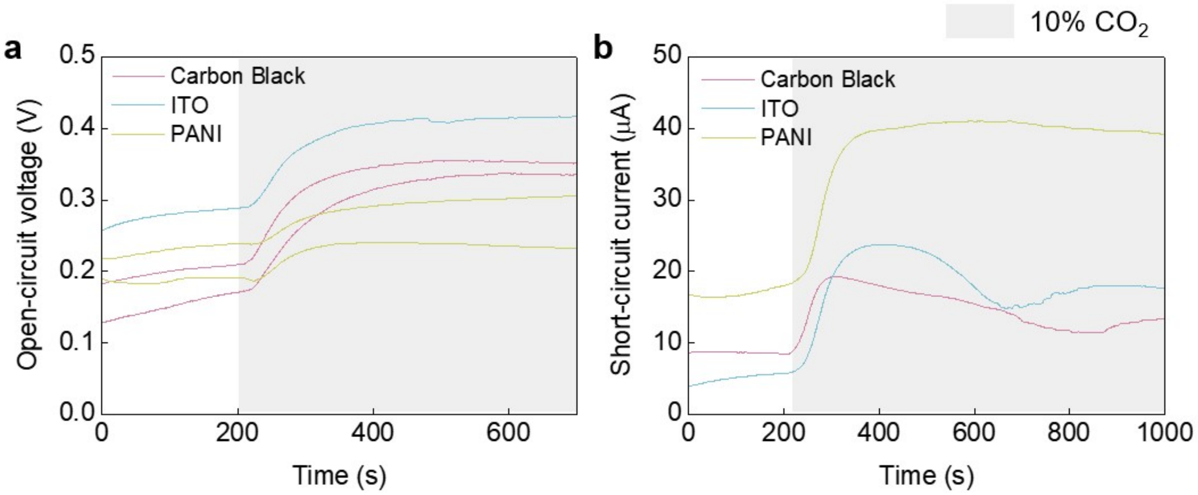

Figure S23. Measured (a) V_{OC} and (b) I_{SC} of the modified-GCEG with different conductive material coatings, exposed to 10% CO_2 at 30% RH.

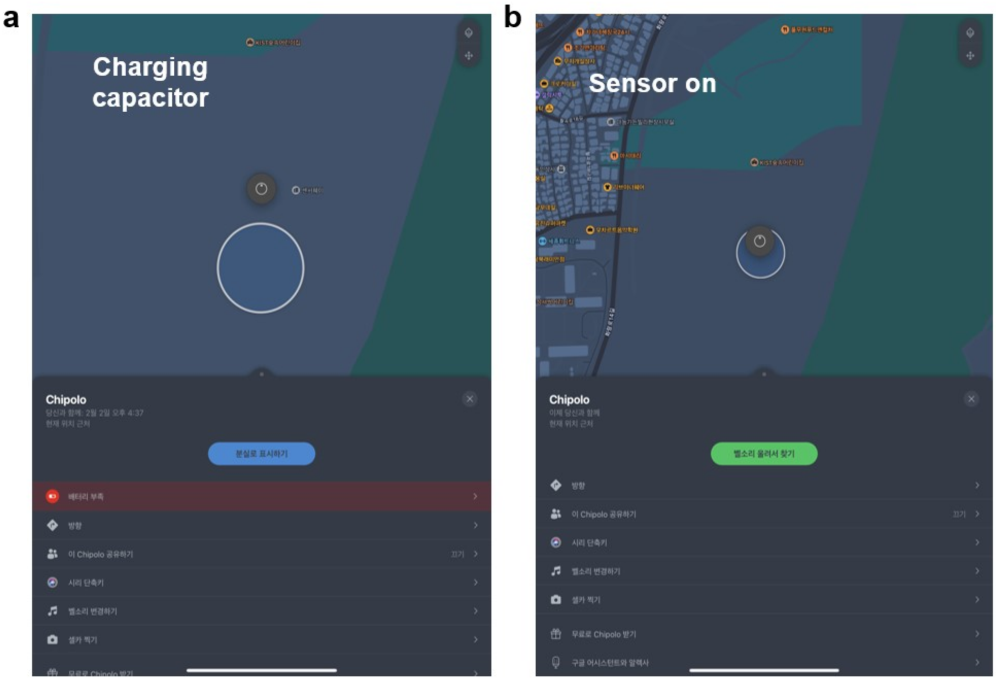

Figure S24. Practical demonstration of an IoT location-tracking sensor powered by the GCEG array, with output displayed on a tablet interface. (a) The IoT device remains off while the capacitor is charging. (b) The sensor is activated once the capacitor discharges.

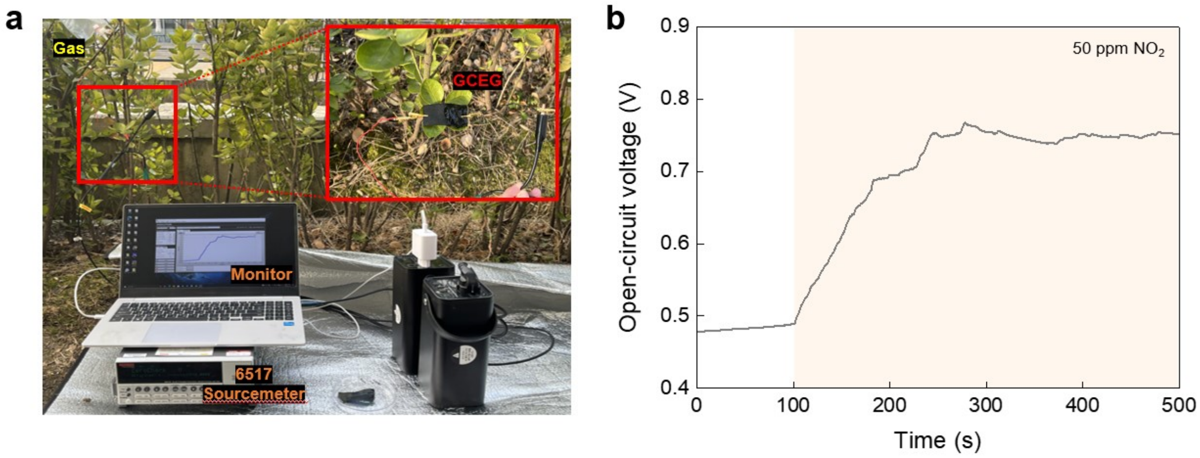

Figure S25. Outdoor performance evaluation of the GCEG. (a) Experimental setup for operating the GCEG under real outdoor conditions. (b) V_{OC} profiles of the GCEG recorded under 50 ppm NO_2 exposure in outdoor conditions.

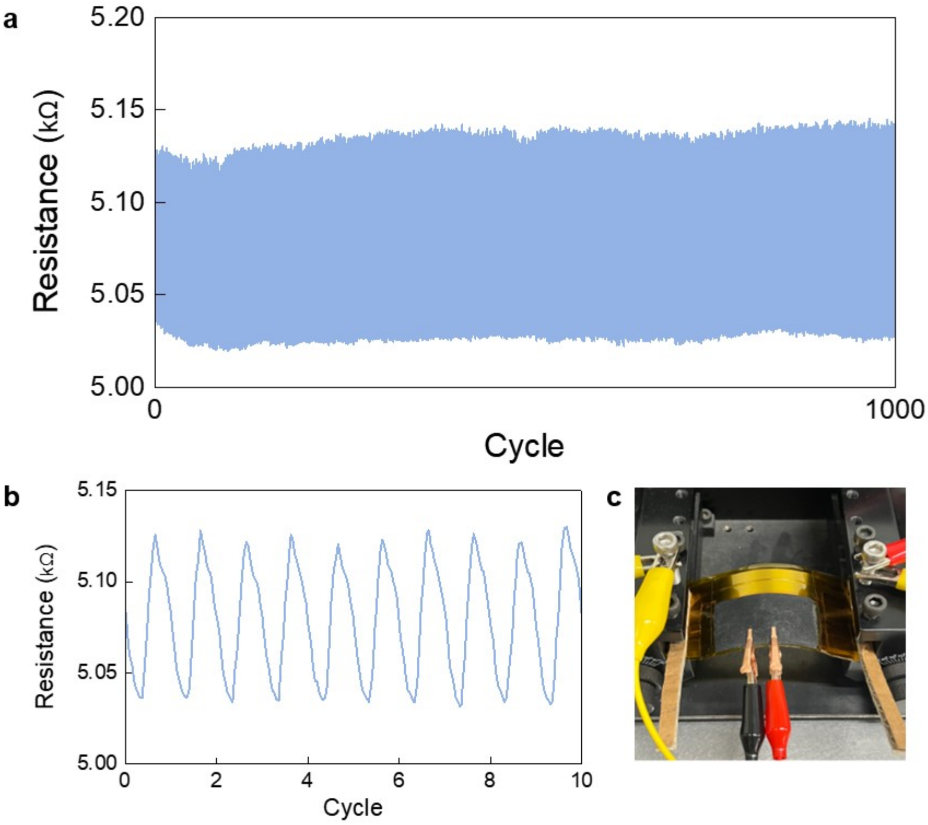

Figure S26. Mechanical durability of carbon black-coated mulberry paper tested under repeated bending. (a) Continuous resistance changes under cyclic bending for 1000 cycles. (b) Resistance measured over 10 bending cycles. (c) Image of the bending test apparatus with the carbon black-coated mulberry paper.

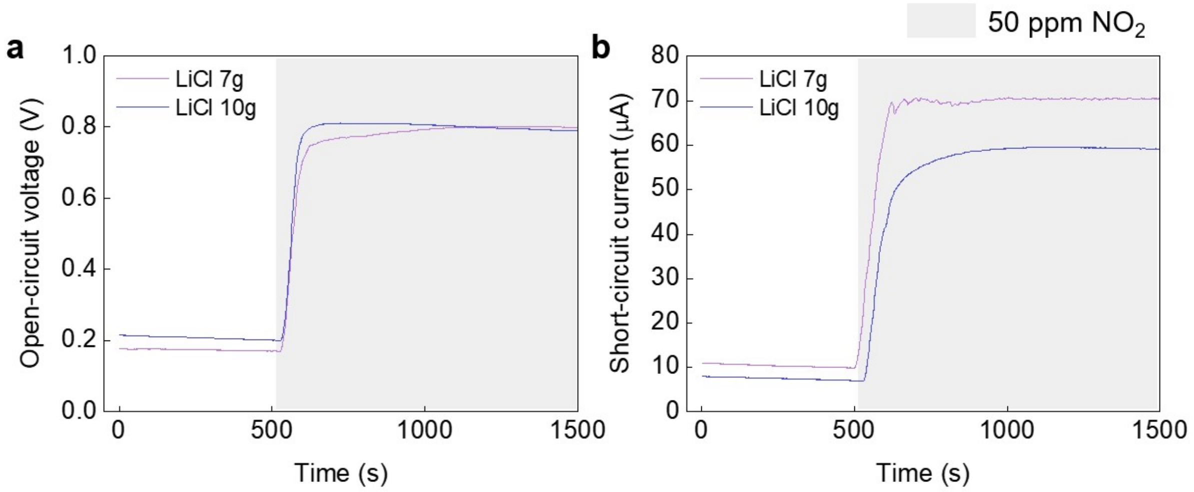

Figure S27. Measured (a) V_{OC} and (b) I_{SC} profiles of the GCEG exposed to 50 ppm NO_2 at 0% RH, as a function of LiCl concentration in the hydrogel.

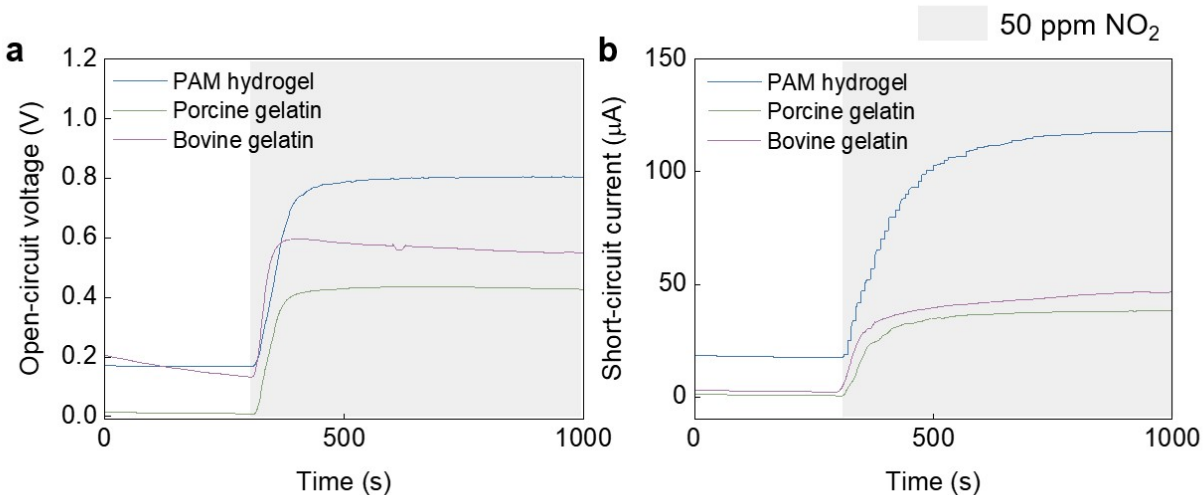

Figure S28. Measured (a) V_{OC} and (b) I_{SC} of the GCEG incorporating porcine and bovine gelatins in place of the PAM hydrogel exposed to 50 ppm NO_2 at 30% RH.

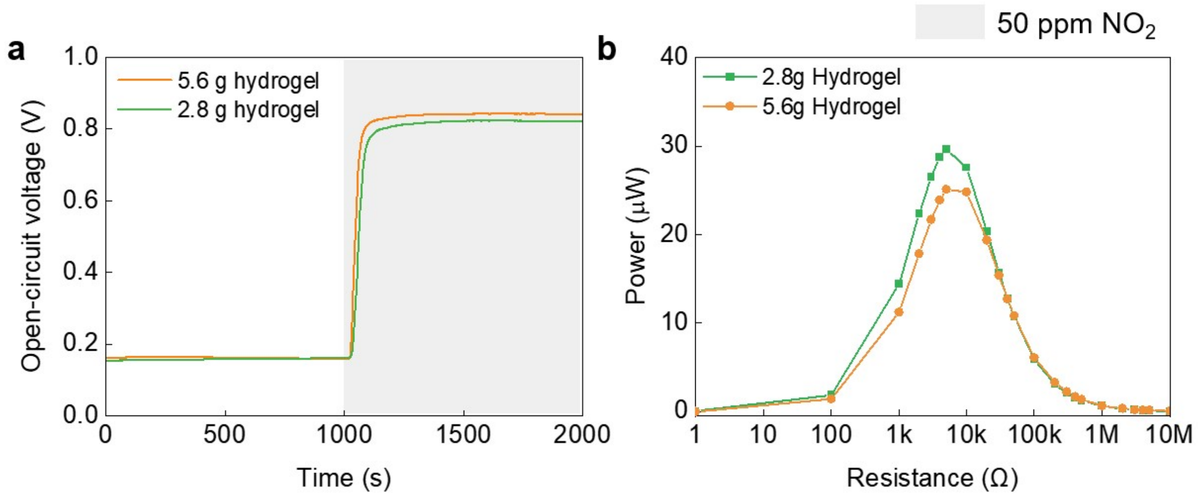

Figure S29. (a) Voltage output and (b) power of the GCEG as a function of hydrogel weight, exposed to 50 ppm NO_2 at 50% RH.

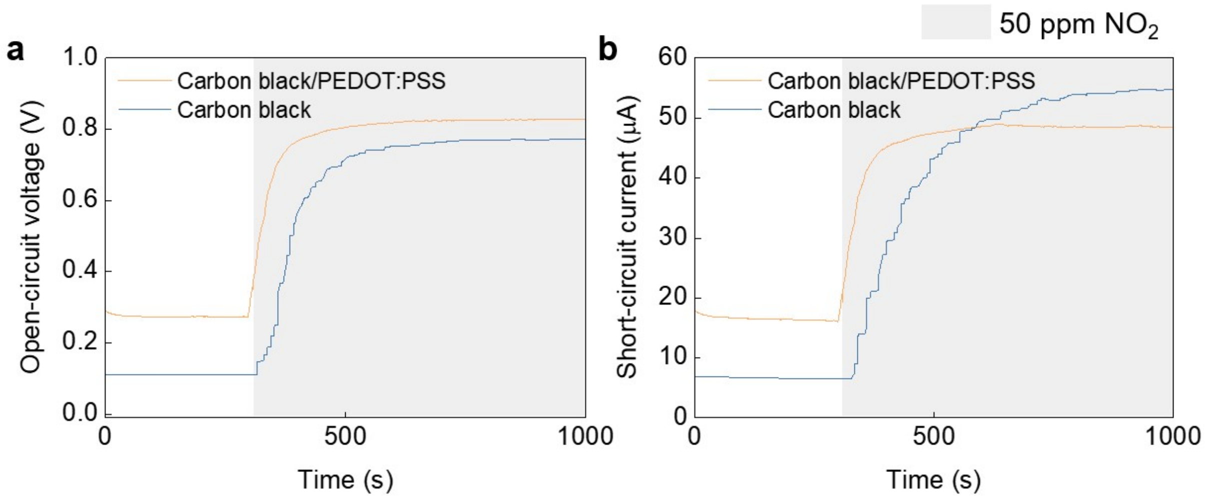

Figure S30. Measured (a) V_{OC} and (b) I_{SC} of the GCEG incorporating a PEDOT:PSS/carbon black(1:1) coating, exposed to 50 ppm NO_2 at 0% RH.

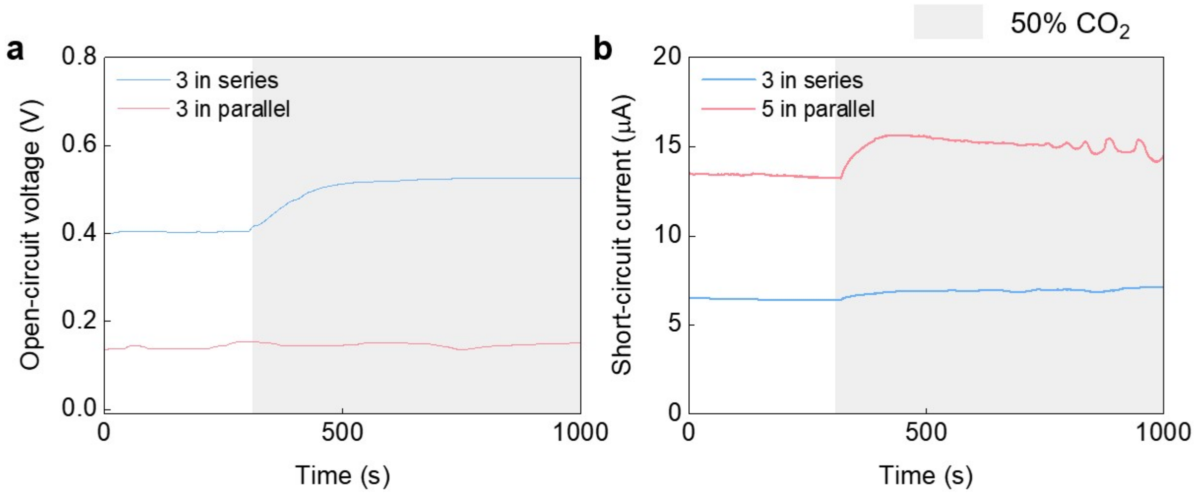

Figure S31. Enhanced (a) voltage and (b) current generation of GCEGs connected in series and parallel, under 50% CO_2 exposure at 50% RH.

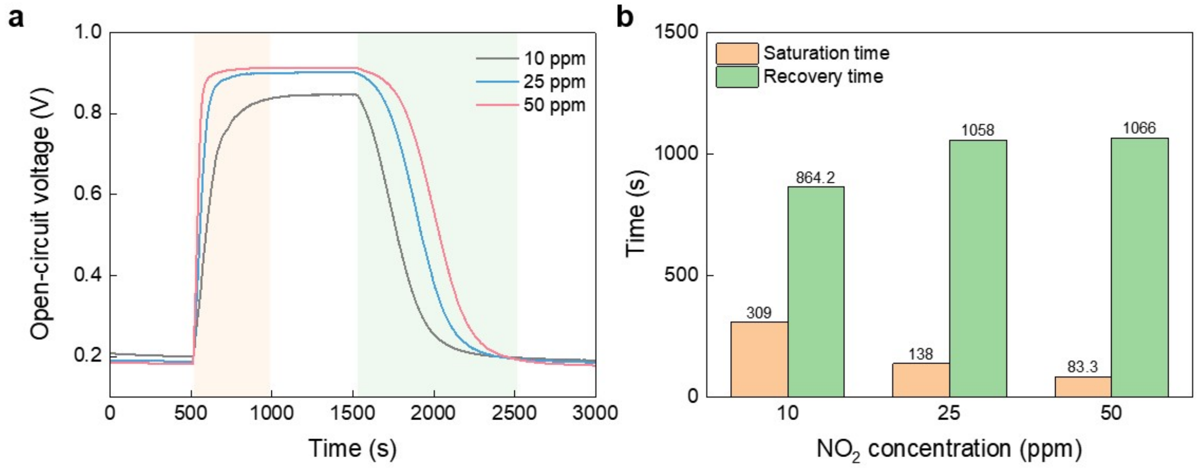

Figure S32. (a) V_{OC} profiles of the GCEG under exposure to 10, 25, and 50 ppm NO_2 at 0% RH, showing the saturation and recovery processes. (b) Calculated saturation and recovery time as a function of NO_2 concentration, where the saturation time is defined as the time elapsed from the gas condition change to the point at which the signal reaches 95% of its steady-state value, and the recovery time as the time elapsed from switching to air until the signal recovers to 95% of its initial baseline value.

Table S1. Comparison of electrical performance with other energy harvesting devices based on electrical double layers.

No.	Method	Material	Voltage	Current	Power	Ref.
1	Water evaporation	Geobacter sulfurreducens biofilms	0.45 V	1.5 μA	1 μW/cm^2	[1]
2	Moisture adsorption	Polyanion hydrogel and polycation hydrogel	0.05 V	0.9 nA	0.36 nW/cm^2	[2]
3	Moisture adsorption and evaporation	Carbon black, LiCl	0.78 V	7.5 μA	0.7 μW/cm^2	[3]
4	Ion diffusion	Sodium alginate, reduced graphene oxide	0.5 V	100 μA	12 μW/cm^2	[4]
5	Moisture adsorption and electromagnetic	P(AAm-co-AAc), PPy (Polypyrrole)	0.59 V	11.45 μA	0.049 μW/cm^2	[5]
6	Moisture adsorption	PEDOT:PSS, PAM/AMPS/LiCl based hydrogel	0.3 V	1.8 μA		[6]
7	Moisture adsorption	Polyacrylonitrile (PAN), NaCl, Polyvinylpyrrolidone (PVP)	0.8 V	14.3 uA/cm^2	0.61 μW	[7]
8	Moisture adsorption	Ketjen black, Polyacrylonitrile (PAN), LiCl	0.24 V	31 μA	9.2 μW/cm^2	[8]
9	Water evaporation	1-n-butyl-3-methylimidazolium chloride (BMIMCl), Cellulose, Polyethylene glycol (PEG)	0.42 V	122.3 μA	11.8 μW/cm^2	[9]
10	Water evaporation	Reduced graphene oxide (rGO)	0.6 V	1.3 μA	0.3456	[10]
This work	Gas energy harvesting	Carbon black, Polyacrylamide hydrogel	0.8 V	55 μA	120 μW	

Table S2. Comparison of NO_2 adsorption capacity with other materials

Classification	**Materials**	**NO_2 adsorption capacity [mmol g^{-1}]**	**Ref.**
Activated carbons (ACs)	Activated carbons from wood	1.43–4.48	11, 12, 13
	Copper-based metal-organic frameworks	4.97–6.70	14
	SBA-15	0.46	15
Silica	Si-60	1.52	16
	13X	2.99	17
Zeolites	4A	0.36	17
	Ni2+SSZ-13-12-L	1.74	18, 19
MOF	HKUST-1	2.30	20
	UiO-66	1.59	21
This work	Carbon black and Polyacrylamide hydrogel	0.17	

Discussion S1. Calculation of gas adsorption capacities.

The gas adsorption capacities were calculated from dynamic breakthrough-type measurements by integrating the difference between the inlet and outlet gas concentrations over time. The total molar amount of gas adsorbed, n_{ads}, is given by

$$n_{ads} = \int_0^{t_s} (n_{in} - n_{out})dt = \int_0^{t_s} \frac{F}{V_m}(C_i - C_o)dt$$

where F is the volumetric flow rate, C_i and C_o are the inlet and outlet gas concentrations (in ppm), respectively, V_m is the molar volume of the gas (24.45 L mol^{-1} at 298 K and 1 atm), and t_s is the saturation time, defined as the time at which the outlet concentration reaches a steady-state value. The gravimetric adsorption capacity q(mmol g^{-1}) was then obtained by normalizing n_{ads} by the mass of the active material w.

For convenience, the above expression can be rewritten as

$$q = \frac{F \cdot C_i}{V_m \cdot w}\left[t_s - \int_0^{t_s} \frac{C_o}{C_i}dt\right]$$

which corresponds to the form used in the present work. The integral term represents the time-integrated fractional breakthrough of the outlet concentration relative to the inlet concentration.

To correct for system-intrinsic transients caused by switching the gas flow path from an empty bypass line to the adsorbent-containing line, a blank correction was applied using an empty adsorbent-containing line under identical conditions. Accordingly, the corresponding term was subtracted from all adsorption measurements to remove this line-switching-induced contribution and to isolate the net gas uptake originating solely form gas-material interactions. The molar volume V_m= 24.45 L mol^{-1} was used based on the experimental conditions (298 K, 1 atm), under which the ideal gas approximation is valid for both NO_2 and CO_2 at the concentrations employed in this study. The calculated adsorption capacities for NO_2 and CO_2 on the bare sample (carbon black-coated mulberry paper), PAM hydrogel and modified GCEG (PAM +DEA), together with the parameters used for calculation, are summarized in Table S#. Representative calculation steps for each case are detailed below.

Table S3. Parameters for calculating gas adsorption capacities.

	Gas	F *(mL min^{-1})*	C_i *(ppm)*	C_o *(ppm)*	w *(g)*	t_s *(min)*	$\int_0^{t_s}\left(\frac{C_o}{C_i}\right)dt$	$\left[t_s - \int_0^{t_s}\left(\frac{C_o}{C_i}\right)dt\right]_{Blank}$	q *(mmol$_{gas}$ g$_{catalyst}^{-1}$)*
Bare	NO_2	0.4	558	558	0.2840	24.85	23.5663	0.32545	0.03
PAM	NO_2	0.4	567	567	1.133	138.08	117.341	0.22545	0.17
Bare	CO_2	0.2	203589	203589	0.0851	7.6286	7.09012	0.41563	2.404

PAM	CO_2	0.2	201140	201140	0.916	329.878	324.05	0.41563	9.721
Modified GCEG	CO_2	0.2	199700	199700	0.8596	1295.91	1281.92	0.41563	25.793

For NO_2,

$$Bare: q = \frac{(0.4 L/min)(558 \times 10^{-6}\, mol/mol)}{24.45\ L/mol \times 0.284\ g}(24.85\ \ min - 23.5663\ min - 0.32545\ min) = 0.03\ \frac{mmol_{NO_2}}{g_{catalyst}}$$

$$PAM\ Hydrogel: q = \frac{(0.4 L/min)(567 \times 10^{-6}\, mol/mol)}{24.45\ L/mol \times 1.133\ g}(138.08\ \ min - 117.341\ min - 0.22545\ min) = 0.17\ \frac{mmol_{NO_2}}{g_{catalyst}}$$

For CO_2,

$$Bare: q = \frac{(0.2 L/min)(203589 \times 10^{-6}\, mol/mol)}{24.45\ L/mol \times 0.0851\ g}(7.6285\ min - 7.09012\ min - 0.41563$$

$$PAM\ hydrogel: q = \frac{(0.2 L/min)(201140 \times 10^{-6}\, mol/mol)}{24.45\ L/mol \times 0.916 g}(329.878\ \ min - 324.05\ min - 0.41563\ min) = 9.721\ \frac{mmol_{CO_2}}{g_{catalyst}}$$

$$Modified\ GCEG: q = \frac{(0.2 L/min)(199700 \times 10^{-6}\, mol/mol)}{24.45\ L/mol \times 0.8596\ g}(1295.91\ min - 1281.92\ min - 0.41563 min) = 25.793\ \frac{mmol_{CO_2}}{g_{catalyst}}$$

References

1. X. Liu, T. Ueki, H. Gao, T. L. Woodard, K. P. Nevin, T. Fu, S. Fu, L. Sun, D. R. Lovley and J. Yao, *Nat. Commun.*, 2022, **13**, 4369.
2. W. Lu, T. Ding, X. Wang, C. Zhang, T. Li, K. Zeng and G. W. Ho, *Nano Energy*, 2022, **104**, 107892.
3. J. Tan, S. Fang, Z. Zhang, J. Yin, L. Li, X. Wang and W. Guo, *Nat. Commun.*, 2022, **13**, 3643.
4. H. Wang, T. He, X. Hao, Y. Huang, H. Yao, F. Liu, H. Cheng and L. Qu, *Nat. Commun.*, 2022, **13**, 2524.
5. Z. Gao, C. Fang, Y. Gao, X. Yin, S. Zhang, J. Lu, G. Wu, H. Wu and B. Xu, *Nat. Commun.*, 2025, **16**, 312.
6. P. Duan, C. Wang, Y. Huang, C. Fu, X. Lu, Y. Zhang, Y. Yao, L. Chen, Q.-C. He and L. Qian, *Nat. Commun.*, 2025, **16**, 239.
7. Z. Sun, X. Wen, S. Guo, M. Zhou, L. Wang, X. Qin and S. C. Tan, *Nano Energy*, 2023, **116**, 108748.
8. P. Li, Y. Hu, W. He, B. Lu, H. Wang, H. Cheng and L. Qu, *Nat. Commun.*, 2023, **14,** 5702.
9. Z. Sun, C. Han, S. Gao, Z. Li, M. Jing, H. Yu and Z. Wang, *Nat. Commun.*, 2022, **13**, 5077.
10. Y. H. Cho, H. Jin, W. H. Lee, J. Han, M. Jin, S. Yu, L. Li, S. G. Yoon and Y. S. Kim, *Nano Energy*, 2023, **118**, 108982.
11. S. Bashkova and T. J. Bandosz, *J. Colloid Interface Sci.*, 2009, **333**, 97-103.
12. B. Levasseur, C. Petit and T. J. Bandosz, *ACS Appl. Mater. Interfaces*, 2010, **2**, 3606-3613.
13. E. Deliyanni and T. J. Bandosz, *Langmuir*, 2011, **27**, 1837-1843.
14. B. Levasseur, C. Petit and T. J. Bandosz, *ACS Appl. Mater. Interfaces*, 2010, **2**, 3606-3613.
15. B. Levasseur, A. M. Ebrahim and T. J. Bandosz, *Langmuir*, 2012, **28**, 5703-5714.
16. A. M. Ebrahim and T. J. Bandosz, *J. Phys. Chem. C*, 2014, **118**, 8982-8992.
17. Z.-M. Wang, T. Arai and M. Kumagai, *Energy Fuels*, 1998, **12**, 1055-1060.
18. F. Delachaux, C. Vallières, H. Monnier and M.-T. Lecler, *Adsorption*, 2019, **25**, 95-103.
19. M. Sun, C. Ku, Z. Tao, T. Wang, C. Wen, A. Hanif, C. Wang, Q. Gu, P. Sit and J. Shang, *Results Eng.*, 2023, **18**, 101134.
20. C. Petit, B. Levasseur, B. Mendoza and T. J. Bandosz, *Microporous Mesoporous Mater.*, 2012, **154**, 107-112.
21. A. M. Ebrahim, B. Levasseur and T. J. Bandosz, *Langmuir*, 2013, **29**, 168-174.